

A single sub-km Kuiper Belt object from a stellar Occultation in archival data

H. E. Schlichting^{1,2}, E. O. Ofek^{1,3}, M. Wenz⁴, R. Sari^{1,5},
A. Gal-Yam⁶, M. Livio⁷, E. Nelan⁷, S. Zucker⁸

October 21, 2009

¹ Department of Astronomy, 249-17, California Institute of Technology, Pasadena, CA 91125, USA

² CITA, University of Toronto, 60 St. George St., ON, M5S 3H8, Canada

³ Einstein Fellow

⁴ Goddard Space Flight Center, 8800 Greenbelt Road, Greenbelt, MD 20771, USA

⁵ Racah Institute of Physics, Hebrew University, Jerusalem 91904, Israel

⁶ Faculty of Physics, Weizmann Institute of Science, POB 26, Rehovot 76100, Israel

⁷ Space Telescope Science Institute, 3700 San Martin Drive, Baltimore, MD 21218, USA

⁸ Department of Geophysics and Planetary Sciences, Tel Aviv University, Tel Aviv 69978, Israel

The Kuiper belt is a remnant of the primordial Solar System. Measurements of its size distribution constrain its accretion and collisional history, and the importance of material strength of Kuiper belt objects (KBOs)[1, 2, 3, 4]. Small, sub-km sized, KBOs elude direct detection, but the signature of their occultations of background stars should be detectable[5, 6, 7, 8, 9]. Observations in both optical[10] and X-ray[11] claim to have detected such occultations, but their implied KBO abundances are inconsistent with each other and far exceed theoretical expectations. Here, we report an analysis of archival data that reveals an occultation by a body with a ~ 500 m radius at a distance of 45 AU. The probability of this event to occur due to random statistical fluctuations within our data set is about 2%. Our survey yields a surface density of KBOs with radii larger than 250 m of $2.1_{-1.7}^{+4.8} \times 10^7 \text{ deg}^{-2}$, ruling out inferred surface densities from previous claimed detections by more than 5σ . The fact that we detected only one event, firmly shows

a deficit of sub-km sized KBOs compared to extrapolation from KBOs with $r > 50$ km. This implies that sub-m sized KBOs are undergoing collisional erosion, just like debris disks observed around other stars.

A small KBO crossing the line of sight to a star will partially obscure the stellar light, an event which can be detected in the star's light curve. For visible light, the characteristic scale of diffraction effects, known as the Fresnel scale, is given by $(\lambda a/2)^{1/2} \sim 1.3$ km, where $a \sim 40$ AU is the distance to the Kuiper belt and $\lambda \sim 600$ nm is the wavelength of our observations.

Diffraction effects will be apparent in the star's light curve due to occulting KBOs provided that both star and the occulting object are smaller than the Fresnel scale [12, 13]. Occultations by objects smaller than the Fresnel scale are in the Fraunhofer regime. In this regime the diffraction pattern is determined by the size of the KBO and its distance to the observer, the angular size of the star, the wavelength range of the observations and the impact parameter between the star and the KBO (see Supplementary Information for details). The duration of the occultation is approximately given by the ratio of the Fresnel scale to the relative velocity perpendicular to the line of sight between the observer and the KBO. Since the relative velocity is usually dominated by the Earth's velocity around the Sun, which is 30 km s^{-1} , typical occultations only last of order of a tenth of a second.

Extensive ground based efforts have been conducted to look for optical occultations [10, 9, 14, 15]. To date, these visible searches have announced no detections in the region of the Kuiper belt (30-60 AU), but one of these quests claims to have detected some events beyond 100 AU and at about 15 AU [10]. Unfortunately, ground based surveys may suffer from a high rate of false-positives due to atmospheric scintillation, and lack the stability of space based platforms. The ground breaking idea to search for occultations in archival RXTE X-ray data resulted in several claimed occultation events [11]. Later, revised analysis of the X-ray data [16, 17, 18, 19] conclude that the majority of the originally reported events are most likely due to instrumental dead time effects. Thus, previous reports of optical and X-ray events remain dubious [14] and their inferred KBO abundance is inconsistent with the observed break in the KBO size distribution, which has been obtained from direct detections of large KBOs [20, 21, 22]. Furthermore, they are also difficult to reconcile with theoretical expectations, which predict collisional evolution for KBOs smaller than a few km in size [23, 4] and hence a lower KBO abundance than inferred from extrapolation from KBOs with

$r > 50$ km.

For the past 14 years, the Fine Guidance Sensors (*FGS*) on board of *Hubble Space Telescope* (*HST*) have been collecting photometric measurements of stars with 40 Hz time resolution, allowing for the detection of the occultation diffraction pattern rather than a simple decrease in the photon count. We examined four and a half years of archival *FGS* data, which contain $\sim 12,000$ star hours of low ecliptic latitude ($|b| < 20^\circ$) observations.

Our survey is most likely to detect occultations by KBOs that are 200–500 m in radius given the signal-to-noise of our data (Supplementary Figure 1) and a power-law size distribution with power-law index between 3 and 4.5. Occultation events in this size range are in the Fraunhofer regime where the depth of the diffraction pattern varies linearly with the area of the occulting object and is independent of its shape. The theoretical light curves for our search algorithm were therefore calculated in this regime. We fitted these theoretical occultation templates to the *FGS* data and performed χ^2 analysis to identify occultation candidates (see Supplementary Information). We detected one occultation candidate, at ecliptic latitude 14° , that significantly exceeds our detection criterion (Figure 1). The best fit parameters yield a KBO size of $r = 520 \pm 60$ m and a distance of 45^{+5}_-4 AU where we assumed a circular KBO orbit and an inclination of 14° . Using bootstrap simulations, we estimate a probability of $\sim 2\%$ that such an event is caused by statistical fluctuations over the whole analyzed *FGS* data set (Supplementary Figure 5). We note that for objects on circular orbits two solutions can fit the duration of the event. However, the other solution is at a distance of 0.07 from the Earth, and is therefore unlikely. It is also unlikely that the occulting object was located in the Asteroid belt, since the expected occultation rate from Asteroids is about two orders of magnitude less than our implied rate. Furthermore, an Asteroid would have to have an eccentricity of order unity to be able to explain the duration of the observed occultation event.

Using the KBO ecliptic latitude distribution from Elliot et. al (2005) [24], our detection efficiency, and our single detection, we constrain the surface density around the ecliptic (averaged over $-5^\circ < b < 5^\circ$) of KBOs with radii larger than 250 m to $2.1^{+4.8}_{-1.7} \times 10^7 \text{ deg}^{-2}$ (see Supplementary Information Sections 5 and 6). This surface density is about three times the implied surface density at 5.5° ecliptic latitude and about five times the surface density at $8 - 20^\circ$ ecliptic latitude. This is the first measurement of the surface density of hecto-meter-sized KBOs and it improves previous upper limits by

more than an order of magnitude [9, 15]. Figure 2 displays our measurement for the sub-km KBO surface density and summarizes published upper limits from various surveys. Our original data analysis focused on the detection of KBOs located at the distance of the Kuiper belt between 30 AU and 60 AU. In order to compare our results with previously reported ground-based detections beyond 100 AU [10], we performed a second search of the *FGS* data that was sensitive to objects located beyond the classical Kuiper belt. Our results challenge the reported ground-based detections of two 300 m-sized objects beyond 100 AU [10]. Given our total number of star hours and a detection efficiency of 3% for 300 m-sized objects at ~ 100 AU we should have detected more than twenty occultations. We therefore rule out the previously claimed optical detections [10] by more than 5σ . This result accounts for the broad latitude distribution of our observations (i.e., $|b| < 20^\circ$) and the quoted detection efficiency of our survey includes the effect of the finite angular radii of the guide stars at 100 AU.

The KBO cumulative size distribution is parameterized by $N(> r) \propto r^{1-q}$, where $N(> r)$ is the number of objects with radii greater than r , and q is the power-law index. The power-law index for KBOs with radii above ~ 45 km is ~ 4.5 [21, 22] and there is evidence for a break in the size distribution at about $r_{\text{break}} \sim 45$ km [20, 21, 22]. We hence use this break radius and assume a surface density for KBOs larger than r_{break} [25] of 5.4 deg^{-2} around the ecliptic. Accounting for our detection efficiency, the velocity distribution of the *HST* observations, and assuming a single power-law for objects with radii less than 45 km in size, we find $q = 3.9_{-0.3, -0.7}^{+0.3, +0.4}$ (1 and 2σ errors) below the break. Our results firmly show a deficit of sub-km sized KBOs compared to large objects. This confirms the existence of the previously reported break and establishes a shallower size distribution extending two orders of magnitude in size down to sub-km sized objects. This suggests that sub-km sized KBOs underwent collisional evolution, eroding the smaller KBOs. This collisional grinding in the Kuiper belt provides the missing link between large KBOs and dust producing debris disks around other stars. Currently our results are consistent with a power-law index of strength dominated collisional cascade [23], $q = 3.5$, within 1.3σ and with predictions for strengthless rubble piles [4], $q = 3.0$, within 2.4σ . An intermediate value of $3 < q < 3.5$ implies that KBOs are strengthless rubble piles above some critical size, $r_c < r < 45$ km, and strength dominated below it, $r < r_c$. Our observations constrain for the first time r_c . At the 2σ level

we find $r_c > 3$ km.

Using our estimate for the size distribution power-law index ($q = 3.9$) and our KBO surface density for 250 m sized KBOs at an ecliptic latitude of $b = 5.5^\circ$, which is the ecliptic latitude of the RXTE observations of Scorpius X-1, we predict that there should be $\sim 3.6 \times 10^9$ 30 m-radius objects per square degree. This is about 150 times less than the original estimate from X-ray observations of Scorpius X-1 that reported 58 events [11], and it is about 30 times less than the revised estimate from the same X-ray observations, which concludes that up to 12 events might be actual KBO occultations [16]. Our results rule out the implied surface density from these 12 events at 7σ confidence level. One can reconcile our results and the claimed X-ray detections only by invoking a power-law index of $q \sim 5.5$ between 350 m and 30 m. More recent X-ray work reports no new detections in the region of the Kuiper belt but places an upper limit of $1.7 \times 10^{11} \text{ deg}^{-2}$ for objects of 50 m in radius and larger [18]. This is consistent with the KBO surface density of $N(> 50 \text{ m}) = 8.2 \times 10^8 \text{ deg}^{-2}$ that we derive by extrapolating from our detection in the hecto-meter size range.

The statistical confidence level on our detection is 98%. However, our conclusions that there is a significant break in the size distribution and that collisional erosion is taking place and the significant discrepancy with previously claimed occultation detections rely on the *low number* of events we discovered. These conclusions would only be strengthened if this event was caused by an unlikely statistical fluctuation or a yet unknown instrumental artifact.

Ongoing analysis of the remaining *FGS* data, which will triple the number of star hours, together with further development of our detection algorithm (i.e., including a larger number of light curve templates) holds the promise for additional detections of occultation events and will allow us to constrain the power-law index of the size distribution further.

- [1] Davis, D. R. & Farinella, P. Collisional Evolution of Edgeworth-Kuiper Belt Objects. *Icarus* **125**, 50–60 January 1997.
- [2] Stern, S. A. & Colwell, J. E. Collisional Erosion in the Primordial Edgeworth-Kuiper Belt and the Generation of the 30-50 AU Kuiper Gap. *Astrophys. J.* **490**, 879–882 December 1997.
- [3] Kenyon, S. J. & Luu, J. X. Accretion in the Early Kuiper Belt. II. Fragmentation. *Astron. J.* **118**, 1101–1119 August 1999.
- [4] Pan, M. & Sari, R. Shaping the Kuiper belt size distribution by shattering large but strengthless bodies. *Icarus* **173**, 342–348 February 2005.
- [5] Bailey, M. E. Can 'invisible' bodies be observed in the solar system. *Nature* **259**, 290–291 January 1976.
- [6] Dyson, F. J. Hunting for comets and planets. *QJRAS* **33**, 45–57 June 1992.
- [7] Axelrod, T. S., Alcock, C., Cook, K. H. & Park, H.-S. in *Robotic Telescopes in the 1990s* (ed Filippenko, A. V.) 171–181 1992).
- [8] Roques, F., Moncuquet, M. & Sicardy, B. Stellar occultations by small bodies - Diffraction effects. *Astron. J.* **93**, 1549–1558 June 1987.
- [9] Zhang, Z.-W., Bianco, F. B., Lehner, M. J., Coehlo, N. K., Wang, J.-H. *et al.* First Results from the Taiwanese-American Occultation Survey (TAOS). *Astrophys. J.* **685**, L157–L160 October 2008.
- [10] Roques, F., Doressoundiram, A., Dhillon, V., Marsh, T., Bickerton, S. *et al.* Exploration of the Kuiper Belt by High-Precision Photometric Stellar Occultations: First Results. *Astron. J.* **132**, 819–822 August 2006.
- [11] Chang, H.-K., King, S.-K., Liang, J.-S., Wu, P.-S., Lin, L. C.-C. *et al.* Occultation of X-rays from Scorpius X-1 by small trans-neptunian objects. *Nature* **442**, 660–663 August 2006.

- [12] Roques, F. & Moncuquet, M. A Detection Method for Small Kuiper Belt Objects: The Search for Stellar Occultations. *Icarus* **147**, 530–544 October 2000.
- [13] Nihei, T. C., Lehner, M. J., Bianco, F. B., King, S.-K., Giammarco, J. M. *et al.* Detectability of Occultations of Stars by Objects in the Kuiper Belt and Oort Cloud. *Astron. J.* **134**, 1596–1612 October 2007.
- [14] Bickerton, S. J., Kavelaars, J. J. & Welch, D. L. A Search for SUB-km Kuiper Belt Objects with the Method of Serendipitous Stellar Occultations. *Astron. J.* **135**, 1039–1049 March 2008.
- [15] Bianco, F. B., Protopapas, P., McLeod, B. A., Alcock, C. R., Holman, M. J. *et al.* A Search for Occultations of Bright Stars by Small Kuiper Belt Objects using Megacam on the MMT. *Astron. J.* **138**, 568–578 August 2009.
- [16] Chang, H.-K., Liang, J.-S., Liu, C.-Y. & King, S.-K. Millisecond dips in the RXTE/PCA light curve of Sco X-1 and trans-Neptunian object occultation. *Mon. Not. R. Astron. Soc.* **378**, 1287–1297 July 2007.
- [17] Jones, T. A., Levine, A. M., Morgan, E. H. & Rappaport, S. Production of Millisecond Dips in Sco X-1 Count Rates by Dead Time Effects. *Astrophys. J.* **677**, 1241–1247 April 2008.
- [18] Liu, C.-Y., Chang, H.-K., Liang, J.-S. & King, S.-K. Millisecond dip events in the 2007 RXTE/PCA data of Sco X-1 and the trans-Neptunian object size distribution. *Mon. Not. R. Astron. Soc.* **388**, L44–L48 July 2008.
- [19] Blocker, A. W., Protopapas, P. & Alcock, C. R. A Bayesian Approach to the Analysis of Time Symmetry in Light Curves: Reconsidering Scorpius X-1 Occultations. *Astrophys. J.* **701**, 1742–1752 August 2009.
- [20] Bernstein, G. M., Trilling, D. E., Allen, R. L., Brown, M. E., Holman, M. *et al.* The Size Distribution of Trans-Neptunian Bodies. *Astron. J.* **128**, 1364–1390 September 2004.
- [21] Fuentes, C. I. & Holman, M. J. a SUBARU Archival Search for Faint Trans-Neptunian Objects. *Astron. J.* **136**, 83–97 July 2008.

- [22] Fraser, W. C., Kavelaars, J. J., Holman, M. J., Pritchett, C. J., Gladman, B. J. *et al.* The Kuiper belt luminosity function from $m(R)=21$ to 26. *Icarus* **195**, 827–843 June 2008.
- [23] Dohnanyi, J. W. Collisional models of asteroids and their debris. *J. Geophys. Res.* **74**, 2531–2554 (1969).
- [24] Elliot, J. L., Kern, S. D., Clancy, K. B., Gulbis, A. A. S., Millis, R. L. *et al.* The Deep Ecliptic Survey: A Search for Kuiper Belt Objects and Centaurs. II. Dynamical Classification, the Kuiper Belt Plane, and the Core Population. *Astron. J.* **129**, 1117–1162 February 2005.
- [25] Fuentes, C. I., George, M. R. & Holman, M. J. A Subaru Pencil-Beam Search for $m(R) \sim 27$ Trans-Neptunian Bodies. *Astrophys. J.* **696**, 91–95 May 2009.
- [26] Skrutskie, M. F., Cutri, R. M., Stiening, R., Weinberg, M. D., Schneider, S. *et al.* The Two Micron All Sky Survey (2MASS). *Astron. J.* **131**, 1163–1183 February 2006.
- [27] Monet, D. G., Levine, S. E., Canzian, B., Ables, H. D., Bird, A. R. *et al.* The USNO-B Catalog. *Astron. J.* **125**, 984–993 February 2003.
- [28] Roques, F., Geogevits, G. & Doressoundiram, A. The Kuiper Belt Explored by Serendipitous Stellar Occultations. *The University of Arizona Press*, 545–556 2008.

Supplementary Information is linked to the online version of the paper at www.nature.com/nature.

Acknowledgments We thank Dr. H. K. Chang for valuable comments that helped to improve this manuscript. Some of the numerical calculations presented here were performed on Caltech’s Division of Geological and Planetary Sciences Dell cluster. Partial support for this research was provided by NASA through a grant from the Space Telescope Science Institute. R. S. acknowledges support from the ERC and the Packard Foundation. A. G. is supported by the Israeli Science Foundation, an EU Seventh Framework Programme Marie Curie IRG fellowship and the Benozio Center for Astrophysics, a research grant from the Peter and Patricia Gruber Awards, and

the William Z. and Eda Bess Novick New Scientists Fund at the Weizmann Institute. S. Z. acknowledges support from the Israel Science Foundation – Adler Foundation for Space Research.

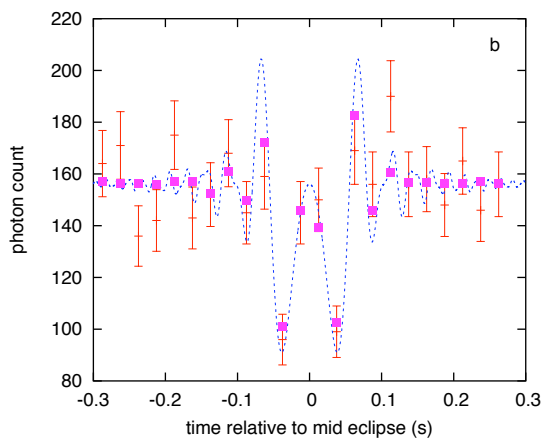
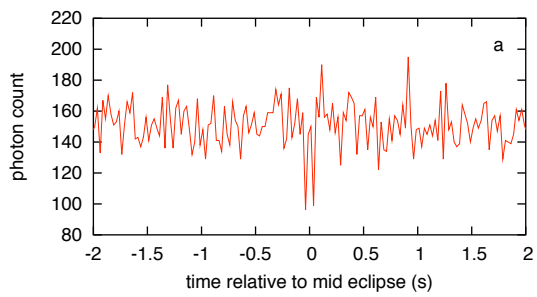
Author Contributions H. E. S. wrote the detection algorithm, analyzed the *FGS* data for occultation events, calculated the detection efficiency of the survey, performed the bootstrap analysis and wrote the paper. E. O. O. calculated the stellar angular radii, the velocity information of the observations, the correlated noise and other statistical properties of the data. R. S. guided this work and helped with the scientific interpretation of the results. A.G. proposed using *HST FGS* data for occultation studies and helped to make the data available for analysis. M. W. extracted the *FGS* photometry streams and provided coordinates and magnitudes of the guide stars. M. L. helped in gaining access to the *FGS* data and provided insights into the operation and noise properties of the *FGS*. E. N. provided expert interpretation of the *FGS* photometric characteristics in the HST operational environment. S. Z. took part in the statistical analysis of the data. All authors discussed the results and commented on the manuscript.

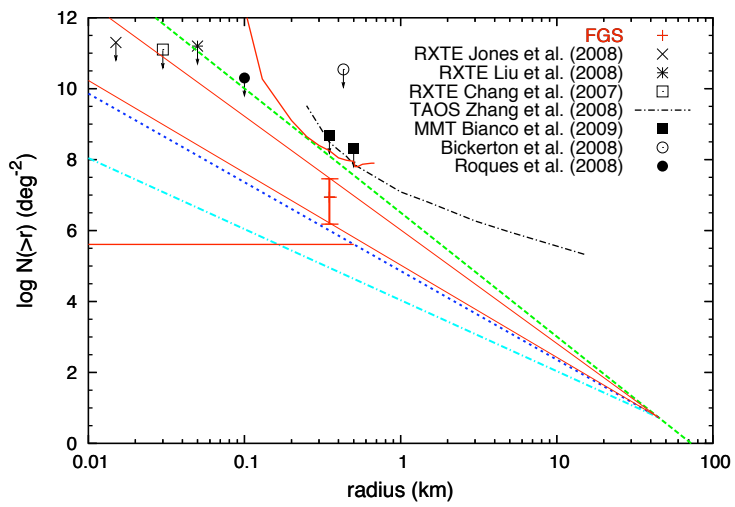
Author Information Reprints and permissions information is available at www.nature.com/reprints. Correspondence and requests for materials should be addressed to H. E. S. (hes@astro.caltech.edu) or E. O. O. (eran@astro.caltech.edu).

Figure 1. Photon counts as a function of time of the candidate occultation event observed by FGS2. Part a) shows the photon count spanning ± 2 seconds around the occultation event. Part b) displays the event in detail. The red crosses and error bars are the *FGS* data points with Poisson error bars, the dashed, blue line is the theoretical diffraction pattern (calculated for the 400-700 nm wavelength range of the *FGS* observations), and the pink squares correspond to the theoretical light curve integrated over 40 Hz intervals. Note, the actual noise for this observation is about 4% larger than Poisson noise due to additional noise sources such as dark counts (about 3 to 6 counts in a 40 Hz interval), and jitter due to the displacement of the guide star (by up to 10 mas) from its null position. The mean signal-to-noise ratio in a 40 Hz interval for the roughly half an hour of observations is ~ 12 . The event occurred at UTC 05:17:49 2007, Mar 24. The best fit χ^2/dof is 20.1/21. The star has an ecliptic latitude of +14. Its angular radius and effective temperature are ≈ 0.3 of the Fresnel scale and ≈ 4460 K, respectively. These values were derived by fitting the 2MASS [26] JHK and USNO-B1 BR [27] photometry

with a black-body spectrum. The position of the star is R.A.=186.87872°, Dec=12.72469° (J2000) and its estimated V-magnitude is 13.4. The auto-correlation function (excluding lag zero) of the photometric time series of this event is consistent with zero within the statistical uncertainty. Each *FGS* provides two independent PMT readings and we confirmed that the occultation signature is present in both of these independent photon counts. We examined the photon counts of the other guide star that was observed by FGS1 at the time of the occultation and confirmed that the occultation signal is only present in the observations recorded by FGS2. We examined the engineering telemetry for *HST* around the time of the event and verified that the guiding performance of *HST* was normal. We therefore conclude that the above occultation pattern is not caused by any known instrumental artifacts.

Figure 2. Cumulative KBO size distribution as a function of KBO radius for objects located between 30 and 60 AU. The results from our *FGS* survey are shown in red and are presented in three different ways: (i) The cross is derived from our detection and represents the KBO surface density around the ecliptic (averaged over $-5^\circ < b < 5^\circ$) and is shown with 1σ error bars. The cross is plotted at $r = 250$ m, which is roughly the peak of our detection probability (see Supplementary Information Section 6 for details). (ii) The upper and lower red curves correspond to our upper and lower 95% confidence level which were derived without assuming any size distribution. (iii) The region bounded by the two straight red lines falls within 1σ of our best estimate for the power-law size distribution index, i.e. $q = 3.9 \pm 0.3$, which was calculated for low ecliptic latitudes ($|b| < 5^\circ$). These lines are anchored to the observed surface density at $r = 45$ km. For comparison, the green (long-dashed) line is the observed size distribution of large KBOs (i.e., $r > 45$ km), which has $q = 4.5$, extrapolated as a single power-law to small sizes. The blue (short-dashed) line is a double power-law with $q = 3.5$ (collisional cascade of strength dominated bodies) for KBOs with radii less than 45 km and $q = 4.5$ above. The cyan (dot-dashed) line corresponds to $q = 3.0$ (collisional cascade of strengthless rubble piles) for KBOs below 45 km in size. All distributions are normalized to $N(> r) = 5.4 \text{ deg}^{-2}$ at a radius of 45 km [25]. In addition, 95% upper limits from various surveys are shown in black. Note, a power-law index of 3.9 was used for calculating the cumulative KBO number density from the RXTE observations.





Supplementary Information

1 The *FGS* Data Set

There are three *FGS* on board of *HST*. Each *FGS* consists of four photomultipliers (PMTs). Nominal *HST* operation uses two *FGS* for guiding, with each *FGS* observing its own guide star. The photon counts recorded by each *FGS* are therefore different, but global instrumental artifacts and Observatory level transients will display in both *FGS* and can therefore be identified and removed.

Observations of the inclination distribution of large KBOs find that about 75% have an inclination angle $|i| \lesssim 20^\circ$ [29, 30, 31]. We therefore divide the *FGS* observations into a low ecliptic latitude ($|b| < 20^\circ$) and a high ecliptic latitude ($|b| > 20^\circ$) sample. The high-ecliptic latitude observations ($|b| > 20^\circ$) provide an excellent control sample.

2 *FGS* Guide Stars

The *FGS* guide stars span a broad range of magnitudes and spectral types. The signal-to-noise ratio, S/N, in a 1/40 s data bin depends on the magnitude of the star. Its distribution is shown in Supplementary Figure 1.

The angular sizes of guide stars were derived by fitting the 2MASS [32] JHK and USNO-B1 BR [33] photometry with a black-body spectrum. Supplementary Figure 2 shows the angular radii distribution of the guide stars. About 66% of the stars in our data set subtend angular sizes less than 0.5 of the Fresnel scale at a distance of 40 AU. The diffraction pattern that is produced by a sub-km sized KBO occulting an extended background star is smoothed over the finite stellar disk. This effect becomes clearly noticeable for stars that subtend sizes larger than about 0.5 of a Fresnel scales [34, 35] and it reduces the detectability of occultation events around such stars. The effect of finite angular radii of the guide stars on the detection efficiency of our survey is taken into account (see Detection Efficiency section 5 for details).

3 Detection Algorithm

Our detection algorithm performs a template search with theoretical light curves and uses a χ^2 fitting procedure to identify occultation candidates. Our survey is most likely to detect KBO occultation events caused by objects that are 200-500 m in radius given the signal-to-noise of our data and for a power-law index of the KBO size distribution, q , between 3 and 4.5. Occultation events in this size range are in the Fraunhofer regime. The theoretical light curves for our search algorithm are therefore calculated in the Fraunhofer regime. Our templates are calculated for various impact parameters assuming a point source background star and are integrated over the 400-700 nm wavelength range of the *FGS* observations. For a given impact parameter between the KBO and the star, our theoretical light curves have three free parameters that we fit for. The first is the mean number of photon counts, which is the normalization of the light curve. The second is the amplitude of the occultation, which is proportional to the size of the KBO, and the third is the width of the occultation, which is independent of the object size, and is determined by the ratio of the Fresnel scale to the relative speed between *HST* and the KBO perpendicular to the line of sight. This relative speed is determined by the combination of *HST*'s velocity around the Earth, Earth's velocity around the Sun and the velocity of the KBO itself. We use this information to restrict the parameter space for the template widths in our search such that we are sensitive to KBOs located at the distance of the Kuiper belt between 30 AU and 60 AU.

4 Detection Criterion and Significance Estimates

The significance of occultation candidates can be measured by their $\Delta\chi^2$ which is defined here as the difference between the χ^2 calculated for the best fit of a flat light curve, which corresponds to no event, and the χ^2 of the best fit template. Occultation events have large $\Delta\chi^2$, since they are poorly fit by a constant. Cosmic ray events, which give rise to one very large photon count reading in a 40 Hz interval, can also result in a large $\Delta\chi^2$ but the fit of the occultation template is very poor. We examined all flagged events for which the template fit of the diffraction pattern was better than 15σ . About a

handful of false-positives where flagged by our detection algorithm that have a value of $\Delta\chi^2$ comparable to or larger than the occultation event. However, in *all* cases these false-positives were caused by jitter due to the displacement of the guide star from its null position. The occultation event itself did not show any such jitter. To determine the $\Delta\chi^2$ detection criterion for our search algorithm and to estimate the probability that detected events are due to random noise we use the bootstrap technique [36]. Specifically, from a given *FGS* time series of length N we randomly selected N points with repetitions and created ‘artificial’ time series from it. We analyzed these ‘artificial’ data sets using the same search algorithm that we applied to the actual *FGS* data. This technique creates random time series with noise properties identical to those of the actual data, but it will lose any correlated noise. Therefore, this technique is justified if there is no correlated noise in the data sets. To look for correlated noise we calculated the auto-correlation function, with lags between 0 to 1 s. Most of the data sets are free of statistical significant correlated noise. The $\sim 12\%$ of the data sets that did show correlated noise exceeding 4σ , which was often due to slopes (e.g., long-term variability) in the data sets, were excluded from the bootstrap analysis.

The *FGS* data set consists of observations of many different stars with magnitudes ranging from 9 to 14. The number of photon counts and signal-to-noise properties vary therefore from observation to observation (see Supplementary Figure 1 for the signal-to-noise ratio distribution of the *FGS* observations). Our $\Delta\chi^2$ calculation accounts for the Poisson noise of the data. Therefore, the probability that occultation candidates are due to random noise can be characterized by a single value of $\Delta\chi^2$ for all observations, irrespective of the mean photon count of a given observation provided that the noise properties across all observations are well characterized by a Poisson distribution. In reality, the noise properties are different from observation to observation; especially non-Poisson tails in the photon counts distribution will give rise to slightly different $\Delta\chi^2$ distributions. Therefore, ideally, we would determine a unique detection criterion for each individual data set. However, this would require to simulate each data set, which contains about an hour of observations in a single *HST* orbit, over the entire length of our survey ($\sim 12,000$ star hours). This is not feasible due to the enormous computational resources that would be required, i.e. simulating a single one hour data set over the entire survey length requires about 5 CPU days, which corresponds to $\sim 60,000$ CPU days for the entire *FGS* survey. Instead, we

perform the bootstrap simulation over all the *FGS* data sets together, where each individual data set was simulated about a 100 times, which required about ~ 500 CPU days in total. This way we estimate the typical $\Delta\chi^2$ value that corresponds to having less than one false-positive detection over the $\sim 12,000$ star hours of low ecliptic observations. For all occultation candidates that exceed this detection threshold, we determined their statistical significance, i.e. the probability that they are due to random noise, by extensive bootstrap simulations of the individual data sets (Supplementary Figure 5).

5 Detection Efficiency

The ability to detect an occultation event of a given size KBO depends on the impact parameter of the KBO, the duration of the event, the angular size of the star and the signal-to-noise ratio of the data. We determined the detection efficiency of our survey by recovering synthetic events that we planted into the observed photometric time series by multiplying the actual *FGS* data with theoretical light curves of KBO occultation events. The synthetic events correspond to KBO sizes ranging from $130 \text{ m} < r < 650 \text{ m}$, they have impact parameters from 0 to 5.5 Fresnel scales and a relative velocity distribution that is identical to that of the actual *FGS* observations. To account for the finite angular sizes of the stars we generated light curve templates with stellar angular radii of 0.1, 0.2, 0.3, 0.4, 0.6, 0.8 and 1 Fresnel scales distributed as shown in Supplementary Figure 2. The modified light curves with the synthetic events were analyzed using the same search algorithm that we used to analyze the *FGS* data. The detection efficiency of our survey was calculated using the angular size distribution of the *FGS* guide stars assuming a distance of 40 AU. We normalize our detection efficiency for a given size KBO, $\eta(r)$, to 1 for an effective detection cross section with a radius of one Fresnel scale.

The detection efficiency of our survey is ~ 0.05 (~ 0.6) for objects with $r = 200 \text{ m}$ ($r = 500 \text{ m}$) located at 40 AU. Note that this value for the detection efficiency already accounts for the angular radii distribution of the guide stars (e.g., for comparison, stars that subtend angular radii less than 0.5 of the Fresnel scale result in a detection efficiency of ~ 0.08 [~ 0.8] for objects with $r = 200 \text{ m}$ [$r = 500 \text{ m}$]).

6 Calculating the KBO Surface Density

The number of occultation events is given by

$$N_{events} \simeq -2v_{rel}F \int_{r_{min}}^{r_{max}} \int_{-b}^b \eta(r) \frac{\Delta t}{\Delta b} \frac{dN(r, b)}{dr} db dr \quad (1)$$

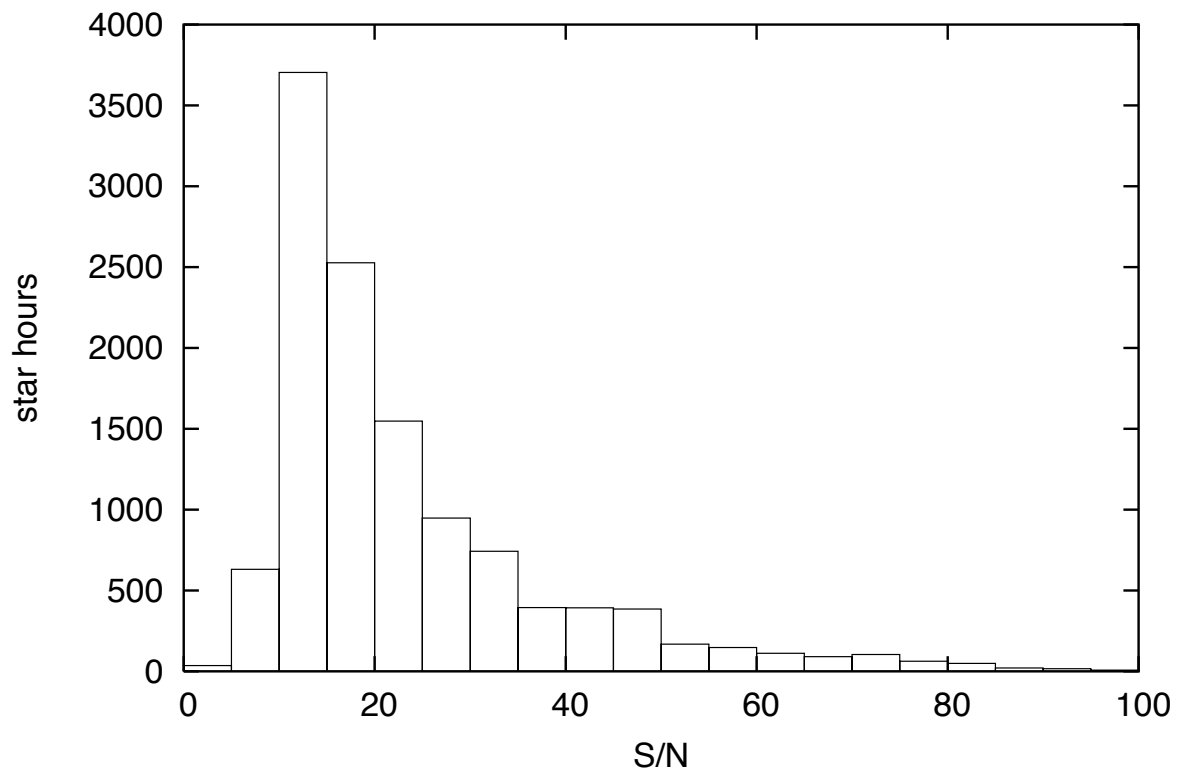
where $v_{rel} = 23$ km/s is the typical relative velocity between the KBO and the observer, b is the ecliptic latitude, $\Delta t/\Delta b$ is the time observed per degree in ecliptic latitude (see Supplementary Figure 3) and $F = 1.3$ km is the Fresnel scale. The number density of KBOs is both a function of ecliptic latitude and the KBO radius, r . Here we assume that the KBO latitude distribution, $f(b)$, is independent of size and we take the distribution provided in Elliot et al. (2005) [31]. We further assume that the KBO size distribution follows a power law. It can therefore be written as $N(r, b) = n_0 \times r^{-q+1} \times f(b)$ where n_0 is the normalization factor for the cumulative surface density of KBOs. Substituting for $dN(r, b)/dr$ in equation 1 and solving for n_0 we have

$$n_0 \simeq \frac{N_{events}}{2v_{rel}F(q-1) \int_{r_{min}}^{r_{max}} \eta(r)r^{-q} dr \int_{-b}^b f(b) \frac{\Delta t}{\Delta b} db} \quad (2)$$

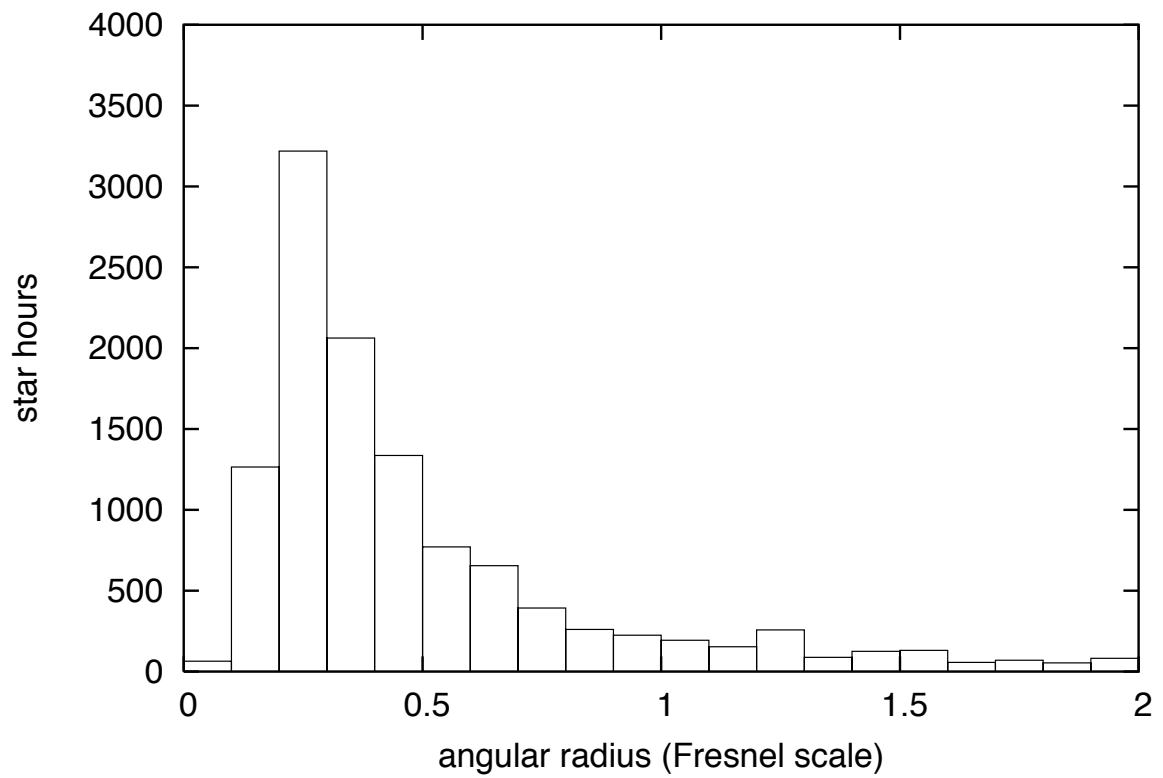
Evaluating equation 2 yields a cumulative KBO surface density averaged over the ecliptic ($|b| < 5^\circ$) of

$$N(r > 250 m) \simeq 2.1 \times 10^7 \text{ deg}^{-2} \quad (3)$$

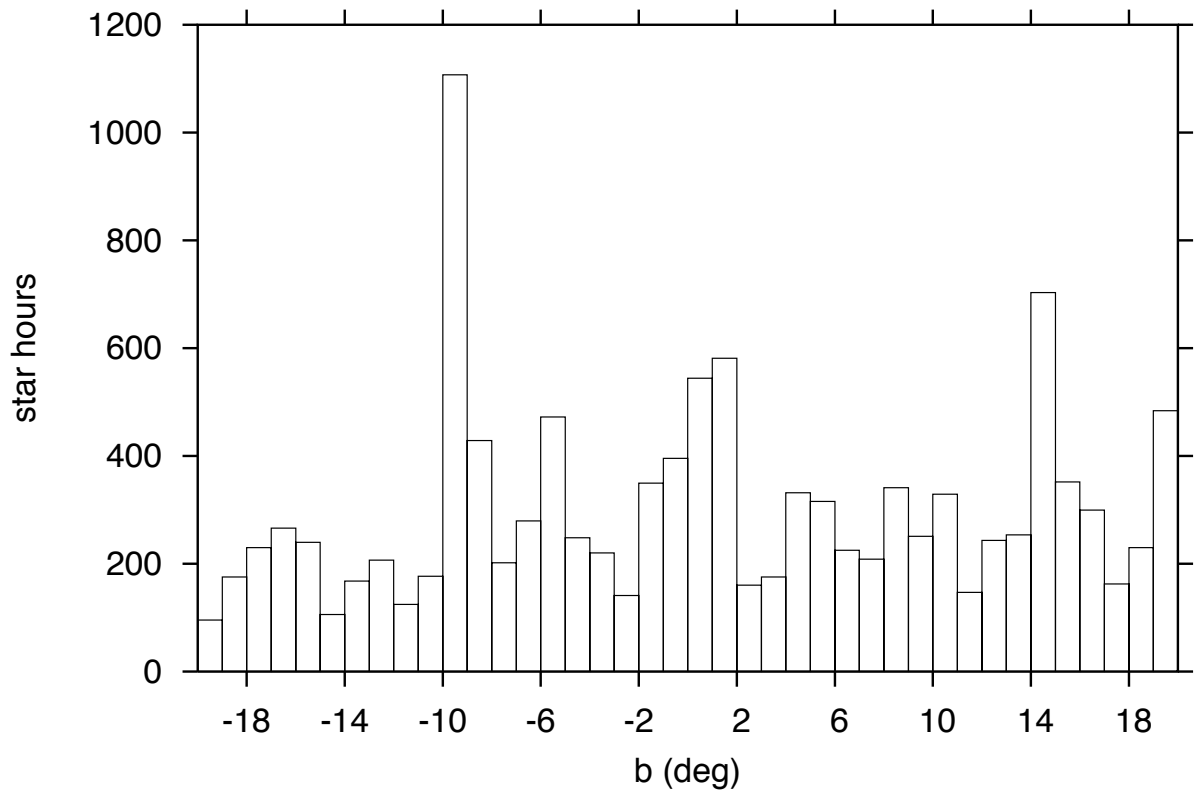
We assumed $q = 4$ when evaluating the integral over r . We note however that the value for the cumulative KBO surface density at $r = 250$ m only depends weakly on the exact choice for q [e.g. $N(r > 250 m)$ only ranges from $2.3 \times 10^7 \text{ deg}^{-2}$ to $2.1 \times 10^7 \text{ deg}^{-2}$ for values of q between 3 and 4.5]. We quote our results as the KBO surface density of objects larger than 250 m in radius since this is roughly the size of KBOs, which our survey is most likely to detect given our detection efficiency and a power-law size distribution with $q = 3 - 4.5$. The implied surface density for KBOs with radii larger than 250 m is $7.7 \times 10^6 \text{ deg}^{-2}$ at $b = 5.5^\circ$, which is the ecliptic latitude of the RXTE observations of Scorpius X-1, and it is $4.4 \times 10^6 \text{ deg}^{-2}$ for $8^\circ < |b| < 20^\circ$.



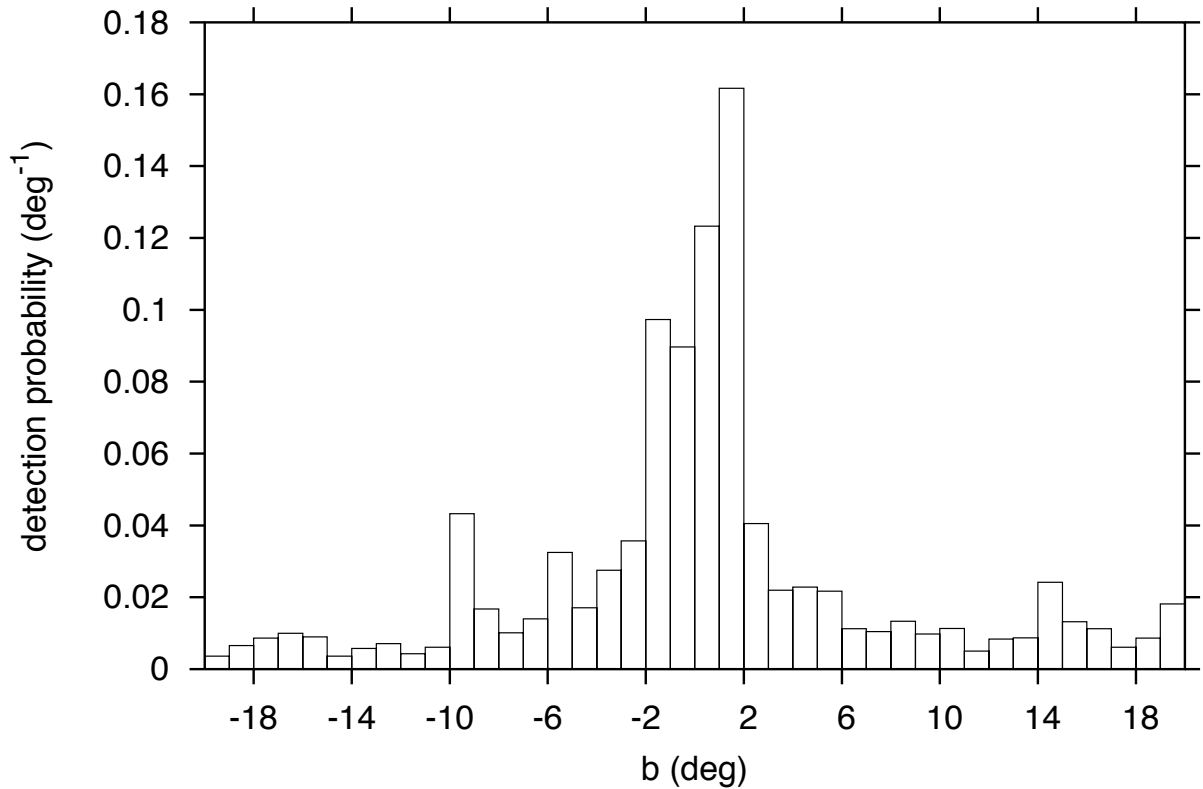
Supplementary Figure 1: Distribution of star hours as a function of the mean signal-to-noise ratio, S/N , in a 40 Hz bin for the 12,000 hours of low ecliptic latitude observations ($|b| > 20^\circ$) in the analyzed FGS data set.



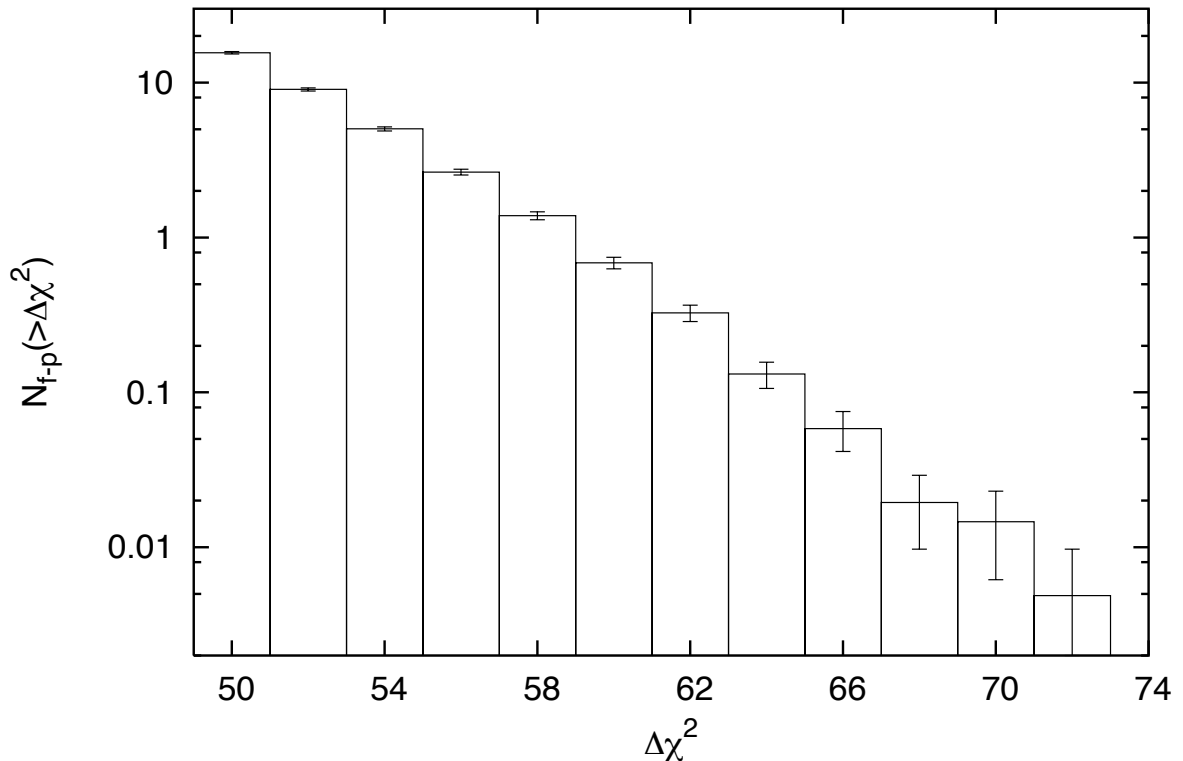
Supplementary Figure 2: Distribution of star hours as a function of angular radii of the guide stars. The angular radii are given as fraction of the Fresnel scale both which are calculated at 40 AU.



Supplementary Figure 3: Distribution of star hours as a function of ecliptic latitude, b , for the 12,000 hours of low ecliptic latitude observations ($|b| > 20^\circ$) in the analyzed FGS data set.



Supplementary Figure 4: Detection probability as a function of ecliptic latitude, b , for the 12,000 hours of low ecliptic latitude observations ($|b| > 20^\circ$) of the analyzed FGS data set. The detection probability was calculated from the ecliptic latitude distribution of FGS guide stars shown in Supplementary Figure 3 and the KBO ecliptic latitude distribution from Elliot et al. (2005)[31]. Note, we assumed that the KBO ecliptic latitude distribution is symmetric about the ecliptic and ignored the small $\sim 1.6^\circ$ inclination of the Kuiper belt plane[31] relative to the ecliptic. For our survey, there is $\sim 60\%$ probability that KBO occultations will occur inside the low-inclination core region ($|b| < 4^\circ$) of the Kuiper belt. The probability for KBO occultations outside the core region is roughly uniform for $4^\circ < |b| < 20^\circ$ and about 40% of all KBO occultations will occur outside the low-inclination core region. The detection of one object at 14° is therefore consistent with the latitude distribution of our observations and that of KBOs.



Supplementary Figure 5: Cumulative number of false-positives, N_{f-p} , as a function of $\Delta\chi^2$. These false-positives were obtained from bootstrap simulations using data from ~ 28 minutes of *FGS* observations that were acquired over one *HST* orbit, in which we discovered the occultation candidate. The original time series was 32 minutes long and we removed the last 4 minutes that showed a significant increasing trend in the number of photon counts. We removed the occultation event itself (which occurred about 2.3 minutes before the start of the trend) and simulated 2.5×10^6 star hours, which is 206 times larger than our low ecliptic latitude observations. This calculation required ~ 1400 CPU days of computing power. The number of false-positives, N_{f-p} , was normalized to 12,000 star hours, which corresponds to the length of the entire low ecliptic latitude observations. In the entire bootstrap analysis we obtained 4 events with a $\Delta\chi^2 \geq 67.3$. This implies a probability of 8×10^{-7} that events like the occultation candidate with $\Delta\chi^2 = 67.3$ are caused by random statistical fluctuations within the original 32 minutes data set that contained the event and a probability of $\sim 4/206 \sim 2\%$ that events like the occultation candidate are caused by random statistical fluctuations over the entire low ecliptic latitude observations. The analysis of our high ecliptic latitude control sample, which is twice as large, did not yield any events that were comparable in significance to the occultation candidate.

Supplementary Information References

- [29] Jewitt, D., Luu, J. & Chen, J. The Mauna Kea-Cerro-Tololo (MKCT) Kuiper Belt and Centaur Survey. *Astron. J.* **112**, 1225–1238 September 1996.
- [30] Brown, M. E. The Inclination Distribution of the Kuiper Belt. *Astron. J.* **121**, 2804–2814 May 2001.
- [31] Elliot, J. L., Kern, S. D., Clancy, K. B., Gulbis, A. A. S., Millis, R. L. *et al.* The Deep Ecliptic Survey: A Search for Kuiper Belt Objects and Centaurs. II. Dynamical Classification, the Kuiper Belt Plane, and the Core Population. *Astron. J.* **129**, 1117–1162 February 2005.
- [32] Skrutskie, M. F., Cutri, R. M., Stiening, R., Weinberg, M. D., Schneider, S. *et al.* The Two Micron All Sky Survey (2MASS). *Astron. J.* **131**, 1163–1183 February 2006.
- [33] Monet, D. G., Levine, S. E., Canzian, B., Ables, H. D., Bird, A. R. *et al.* The USNO-B Catalog. *Astron. J.* **125**, 984–993 February 2003.
- [34] Roques, F. & Moncuquet, M. A Detection Method for Small Kuiper Belt Objects: The Search for Stellar Occultations. *Icarus* **147**, 530–544 October 2000.
- [35] Nihei, T. C., Lehner, M. J., Bianco, F. B., King, S.-K., Giammarco, J. M. *et al.* Detectability of Occultations of Stars by Objects in the Kuiper Belt and Oort Cloud. *Astron. J.* **134**, 1596–1612 October 2007.
- [36] Efron, B. *The Jackknife, the Bootstrap and other resampling plans*. Society for Industrial Mathematics (1982).